



Research article

Wood cellulose fibers reinforced polylactic acid composite: mechanical, thermomechanical characteristics and orientation of fiber

Usman Saeed*

Department of Chemical and Materials Engineering, Faculty of Engineering King Abdulaziz University, Jeddah, Saudi Arabia

* **Correspondance:** Email: usman144de@yahoo.com.

Abstract: The wood cellulose fiber (WCF) reinforced polylactic acid (PLA) offers cost effectiveness, ease of mass production, short processing time, structural stability, high quality and efficient recyclability. In the study presented orientation of fiber, microstructure and thermomechanical property of composites are being examined by using X-ray tomography, scanning electron microscopy (SEM), and dynamic mechanical thermal analysis (DMA). Also, the mechanical properties of WCF–PLA–MAH composites were characterized and analyzed. The results demonstrated that the best outcome of elastic modulus and tensile strength were accomplished at 30%WCF–PLA–3%MAH composite. The DMA result explains that by adding MAH in WCF–PLA as an interfacial coupling agent enhanced the storage modulus and increased the toughness of WCF–PLA composite by decreasing the $\tan\delta$ peak. X-ray tomography of the PLA/WCF/FB composite shows that the degree of anisotropy is accomplished 25% higher when WCF was 30% in PLA matrix. In addition, the SEM micrograph shows that when MAH was used the interfacial compatibility between the PLA matrix and WCF improved.

Keywords: polylactic acid (PLA); wood cellulose fiber (WCF); maleic anhydride (MAH); dynamic mechanical analysis (DMA); X-ray Tomography; degree of anisotropy (DA)

1. Introduction

Today the emphasis on studying the physical characteristics of biodegradable and sustainable materials have become a priority as their use reduces the impact of manufactured products on environment. The applications of sustainable material are in high demand in the fields of packaging,

automotive, biomedical and structural engineering [1–3]. The naturally found chitosan, cellulose and lignin are being studied to find their suitability in diverse application in the field of product design, engineering and mass production [4–6].

The polylactic acid (PLA) as a matrix of composite has attracted attention due to its high impact resistance, mechanical strength and chemical resistance [7–10]. Also, the corn starch, tapioca roots, sugar cane and sugar beet are replenishable resources from where the PLA is mostly sourced. Moreover, PLA is a linear aliphatic thermoplastic with high quality biocompatibility, non-toxic by-products formation and superb transparency. The use of PLA can be found in industries such as packaging, textile and automotive. However, there are drawbacks which limit its use such as low glass transition temperature and high cost. The enhancement in the production of bio composites is made by addition of natural fibers which are being utilized as reinforcing fiber. A vast array of natural fiber such as rice, husk, jute, flax [11–13], cellulose acetate [14] and wood cellulose [15] have been examined in the development of PLA composite.

The cost effective wood cellulose fiber has been preferred and studied in the field of engineering as reinforcement. The structure of cellulose consists of small semicrystalline crystals and microfibrils which are randomly positioned in matrix. Moreover, the properties of wood cellulose also include thermal stability, higher stiffness and strength. The studies done previously have shown that the wood cellulose fiber when applied in engineering is capable of enduring externally applied forces due to its intertwined network [16–18]. The useful characteristics of the wood cellulose fibers which can be utilized include 0.1 ppm/K coefficient of thermal expansion, 114 GPa Young's modulus, 89% degree of crystallinity and 37 m²/g specific surface area [19–20]. The challenges faced during the reinforcement of PLA with wood fiber can be poor compatibility. The study work concentrates on improving the compatibility between wood fiber and PLA matrix by using coupling agent which can enhance the interfacial bonding at the interfaces [21]. Furthermore, the beneficial characteristics and sustainability of natural fiber reinforced polylactic acid makes it a preferential material when compression molding is being used.

The analysis of damping and its effect on composite can be determined by using dynamic mechanical analysis (DMA) technique. The technique is helpful in assessing the time, atmosphere, stress, temperature and function of frequency. The structure of composite can be studied by using dynamic mechanical response with the application of micromechanics and constitutive models. The results of DMA are based on phases in polymer blends, interfaces between matrix and fiber, morphology and the composition of constituents [22–23]. Moreover, the results of DMA show that the composite is strongly influenced by the fiber content, mode of testing, coupling agent and orientation of fiber [24]. The researchers have demonstrated the DMA results in the form of loss tangent ($\tan\delta$) and storage modulus (G') for sisal fiber, jute fiber, wood particles and cellulose triacetate fiber in polymer matrix. The Loss tangent ($\tan\delta$) and storage modulus (G') of the composite are completely dependent on fiber content, orientation and compatibility [23–26].

The X-ray tomography is being applied commonly for applications in medicine and medical diagnostics [27–28]. Furthermore, X-ray tomography is also being utilized to examine the internal structure of specimen [29]. Pandita and Verpoest [30] computed the stiffness of fabric composite by utilizing Tomography technique. Faessel et al. [31] has examined the correlation between thermal conductivity and microstructure of network by using 3D modeling. Also, the X-ray tomography was utilized to investigate the structure of wood fiber reinforced composites [32–36].

The aim of the intended investigation is to explore the performance of wood cellulose fiber

(WCF) reinforced polylactic acid (PLA) composite. The study was conducted by examining mechanical properties, dynamic mechanical properties and orientation of fibers. The Maleic anhydride is also being used as a compatibilizer and coupling agent in the WCF reinforced PLA composite.

2. Materials and methods

2.1. Preparation of material

Nature Works, USA provided the PLA 2003D having melt flow index of 6 g/10 min. American Wood cellulose fibers supplied 12020 grade wood cellulose fiber (WCF) having 20 μm dia and fiber length in the range of $0.1 \leq LW \leq 0.2$ mm. DuPont Canada provided the Maleic Anhydrid having melt flow index of 2 g/10 min which is used as coupling agent. The wood cellulose fibers with variable content of 10%, 20% and 30% having 1% to 3% Maleic anhydride, as shown in Table 1, were utilized to develop the WCF–PLA composite. The components of the product were blended by using co-rotating twin-screw extruder (Liestritz model ZSE27). The extrusion of the mixture was carried out at temperature of 210 °C with screw speed of 80 rpm. The obtained pellets were compression molded at 160 °C by using Carver Hydraulic press to obtain the desired standard geometry of specimen.

Table1. Composition of PLA/WCF/MAH composite.

S.NO	PLA (wt%)	WCF (wt%)	% MAH (wt%)
1	100	-	-
2	90	10	-
3	80	20	-
4	70	30	-
5	89	10	1
6	79	20	1
7	69	30	1
8	87	10	3
10	77	20	3
11	67	30	3

2.2. Mechanical properties

The Tensile Testing machine (Instron, USA) of 50 kN with load accuracy of 0.01% was utilized for tensile tests. The test was carried out having cross head speed of 10mm/min for compression molded specimen having geometry of ASTM D638 type IV. The three samples for each composition were tested at 25 °C.

The JB W300J impact testing machine (Test lab, Poland) was employed for Charpy impact test. The sample dimensions were 10 mm \times 10 mm \times 55 mm with 2 mm notch size according ASTM D256. The 5.2 m/s, 150 ± 1 J, 150° were impact speed, potential impact energy and raise angle of testing machine to perform the impact test respectively.

2.3. Dynamic mechanical analysis

The storage modulus G' and loss factor ($\tan\delta$) of the specimens were determined by employing DMA 242 (Netsch, Germany) using dual cantilever in the temperature range of 25 to 120 °C. The specimen dimensions were 40 mm × 12 mm × 5 mm. The test was carried out at a strain rate of 0.1% and frequency of 1 Hz with the heating rate of 2 °C/min.

The DMA 242 (Netsch, Germany) was also employed to perform the stress relaxation tests in tension mode by using applied strain of 0.8% at 25 °C for 45 min. The specimen dimensions were 40 mm × 12 mm × 5 mm.

2.4. Scanning electron microscope

The field emission scanning electron microscope, JEOL JSM-7600F (Peabody, MA) was utilized to examine the fracture surface morphology of the PLA/WCF/MAH composites at an accelerating voltage of 10 kV.

2.5. X-ray tomography

The high resolution SkyScan-1172 X-ray micro tomography was used for the images of selected area of specimen as shown in Figure 1a. The X-ray source cone beam without filter was aligned at 25 keV and 140 mA beam current. The rotation of samples was done in increments of 0.4° in a range of 180°. The resolution of camera was 4000 × 2300 pixels with Voxel resolution of 10 μm. The software N Recon based on FeldKamp algorithm was used to reconstruct the images. The parameters stayed constant during the characterization of specimen and image reconstruction. The reconstruction of images helped in recognition by choosing from variety of threshold. The variety of threshold appears due to the difference in absorption capability of WCF and PLA. The threshold algorithm was used for segmentation of fiber and segmented fibers were evaluated over the entire reconstructed volume of the micro tomographed sample of 386 × 323 × 424 voxel³. The threshold was set to the value considering a fiber volume/total volume (FV/TV) ratio which corresponds to the volumetric fiber fraction of the composite.

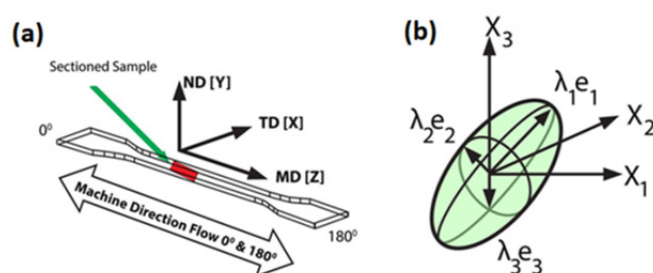


Figure 1. (a) schematic design of the compression molded plate and the position of the sample collected for the X-ray micro tomography experiments (0° and 180° is the same direction), (b) 3D ellipsoid is projected onto the plane of each element to produce a plane ellipse [37]. ND: normal direction (Y axis); TD: transverse direction (X axis); MD: machine direction (Z axis).

The orientation of fiber was studied by using mean intercept length (MIL) concept, as described in previous publication [37], of exposed reconstructed and segmented volume which is considered as Volume of Interest (VOI). The fiber orientation in each selected section was estimated by showing an elliptical image of fiber. The ellipsoid of orientation is being presented in the Figure 1b. The ellipsoid explained a tensor of second order having eigen values of $\lambda_1, \lambda_2, \lambda_3$ and the eigenvectors of $e_1, e_2,$ and e_3 related to fiber orientation [37]. The eigen values and eigenvectors of the orientation tensor are created for graphical demonstration. The eigen vectors demonstrate the most noticeable directions of fiber alignment. Also, the Eigen values provide the statistical proportions from 0 to 1 of fibers lining up (alignment) with the corresponding directions. The graphical representation with the help of eigen values and eigen vector describes the orientation and alignment of fiber.

The Eq 1a presents the tensor of second-order having principle components:

$$a_{ij} = \begin{bmatrix} a_{11} & a_{12} & a_{13} \\ a_{21} & a_{22} & a_{23} \\ a_{31} & a_{32} & a_{33} \end{bmatrix} \quad (1a)$$

a_{ij} indicates the tensor of second order for fibers. Furthermore, with attained Eigen value the related eigenvectors fits the Eq 1b

$$a_{ij} = \begin{bmatrix} \lambda_1 & 0 & 0 \\ 0 & \lambda_2 & 0 \\ 0 & 0 & \lambda_3 \end{bmatrix}; \lambda[e_1 + e_2 + e_3] \quad (1b)$$

The eigenvectors are found to be related with the direction of anisotropic structure.

3. Results and discussion

3.1. Mechanical properties

The Figure 2a,b demonstrates the tensile strength and % elongation at break while Figure 2c,d shows the modulus and impact strength of WCF/PLA/MAH composite. It can be observed from Figure 2a,b that the addition of WCF in PLA matrix enhances the tensile strength and also reduces the elongation at break. The tensile strength improved up to 44.3 MPa and the % elongation at break reduced to 14.6% when 30% WCF was added in PLA. The addition of 3% MAH in the 30%WCF–PLA improves the tensile strength by 8% (46.7 ± 3 MPa) and decreases the % elongation at break by 10% when compared to MAH free WCF–PLA composite. The improvement in strength and reduction in % elongation in the WCF–PLA–MAH composite characteristic can be associated to the similarity found in the PLA molecular chain and MAH polar molecule [38]. Zhang et al. [39] found the results that the strength of the PLA/30%WF/MAH composite reaches up to 48.5 MPa which correspond to the presented results. The addition of MAH in WCF–PLA composite align the interfaces coherently when external forces are applied showing efficient transfer of stress from PLA matrix to wood cellulose fiber. The effective stress distribution improves the tensile strength of WCF–PLA–MAH composite when compared to MAH free WCF–PLA. Furthermore, the effect of improved characteristics by addition of MAH in WCF–PLA is visible in enhancement of tensile strength when compared to WCF–PLA composite where MAH is absent. In addition, it can be observed in Figure 2c,d that the impact strength is reduced up to 3.81 kJ/m² and the elastic modulus

is improved by 1.08 GPa when 30%WCF is added in PLA. The reduction in impact strength and improvement in elastic modulus occurs because of the presence of WCF which hinders the motion of PLA chains. Moreover, the impact strength of composite is improved by 5.29 kJ/m² and modulus is improved by 1.17 GPa when 30%WCF–PLA composite contains 3%MAH. The enhancements show that the impact strength improved by 7% and the modulus increased by 10% when compared to MAH free WCF–PLA composite. The increase in interfacial compatibility and stability of WCF–PLA–MAH composite shows that interfacial adhesion improved due to the presence of MAH anhydride group and hydroxyl group in PLA matrix. Also, the impact strength and modulus improvements during the process of compression molding demonstrate the development of cross linking in the WCF–PLA–MAH composite.

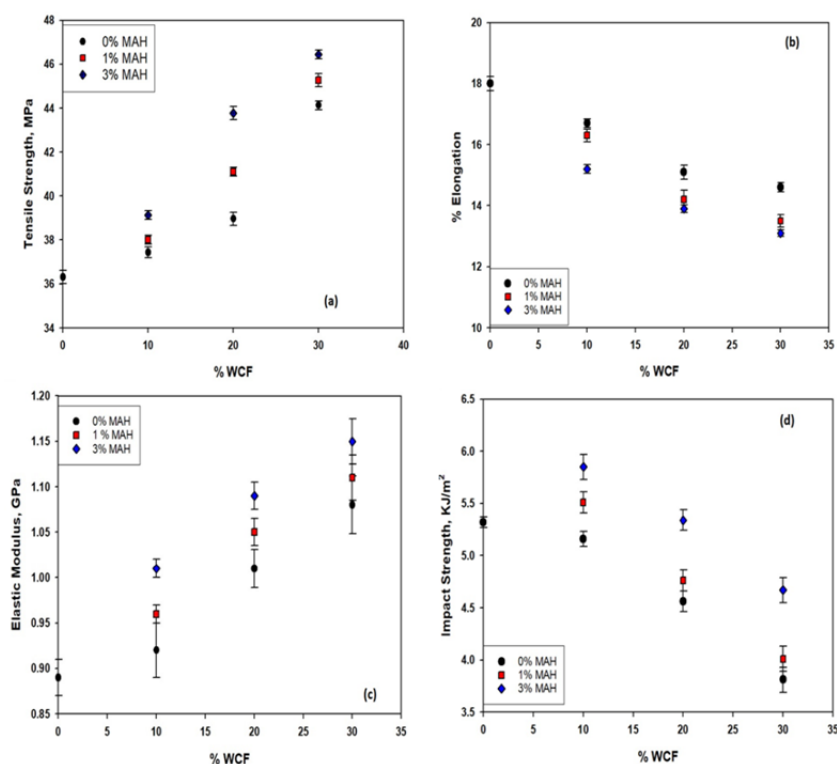


Figure 2. Mechanical properties of PLA–WCF–MAH composites (a) tensile strength, (b) % elongation at break, (c) elastic modulus, and (d) impact strength.

3.2. Stress relaxation

The stress relaxation of WCF–PLA–MAH composite is illustrated in Figure 3. The rate of stress relaxation shows the changes in stress relaxation modulus. In the initial stage the stress relaxation modulus decreases intensely and afterwards decreases gradually indicating the limits of stress relaxation. The outcome of Figure 3a shows that when stresses are applied the neat PLA relaxed 20%, 10%WCF–PLA relaxed 14%, 20%WCF–PLA relaxed 11% and 30%WCF–PLA relaxed 8%. The inclusion of 30% WCF in PLA resulted in the increase of stress relaxation period when compared to neat PLA. The relaxation modulus and delayed stress relaxation are the result of hindrance in motion of PLA chains due to the presence of WCF in PLA matrix. The presence of WCF hinders the

reorientation and restricts the PLA chains mobility. The observation shows that the stress relaxation can be lowered when more WCF is added [40]. Figure 3b illustrates the addition of MAH in 20%WCF–PLA. The addition of 3% MAH in 20%WCF–PLA composite decreases the stress relaxation up to 8% when compared to MAH free composite. The addition of MAH in WCF–PLA has significant effect on stress relaxation because of interfacial bond formation and increase in interfacial surface area. Moreover, the presence of MAH assists in increasing the shear stress at the interface of WCF–PLA composite because of homogenous load transfer. The significant values of relaxation modulus for the PLA, PLA–WCF, and PLA–WCF–WCF composites are presented in Table 2.

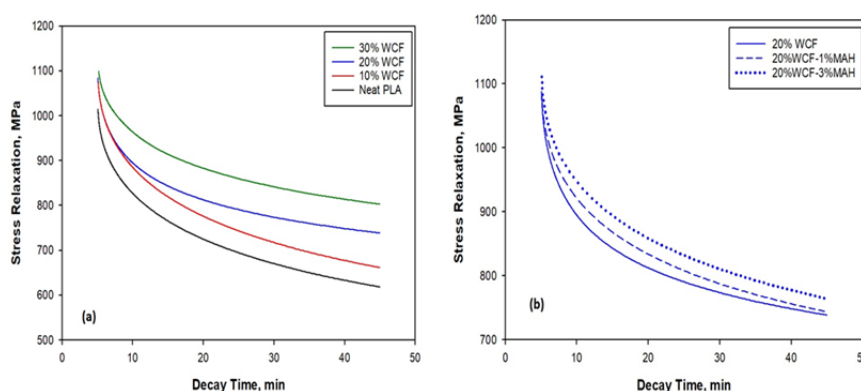


Figure 3. Stress relaxation behavior (a) WCF–PLA composites (b) 20%WCF–PLA–MAH.

Table 2. Relaxation modulus, storage modulus, G' , $\text{Tan}\delta$, glass transition temperature T_g and adhesion factor A , of PLA–WCF–MAH composite.

PLA–WCF–MAH (wt%)	Relaxation modulus (MPa)	Storage modulus G' (MPa)	$\text{Tan}\delta$ peak height	T_g ($^{\circ}\text{C}$)	Adhesion factor “A”
100/0/0	1015.10 ± 1.13	3450	1.81	56.13	-
90/10/0	1083.20 ± 2.01	3622	1.62	58.87	-0.26
80/20/0	1084.48 ± 1.83	3701	1.58	58.93	-0.35
70/30/0	1091.22 ± 1.74	4011	1.21	59.98	-0.43
89/10/1	1092.37 ± 2.23	3673	1.52	60.71	-0.41
79/20/1	1099.63 ± 2.31	3753	1.45	60.34	-0.45
69/30/1	1119.29 ± 1.34	4047	1.09	60.69	-0.49
87/10/3	1097.14 ± 1.91	3711	1.47	61.23	-0.54
77/20/3	1111.80 ± 1.53	3801	1.18	61.43	-0.57
67/30/3	1191.33 ± 1.11	4101	0.81	61.76	-0.61

3.3. Thermomechanical properties

The Figure 4a demonstrates the storage modulus (G') of PLA and WCF–PLA composites. The addition of 30% WCF in PLA increases the storage modulus from 3450 to 4050 MPa which is 15% increased when compared to neat PLA. The 15% increase in storage modulus of 30%WCF/PLA is due to the wood cellulose fiber acting as barrier in PLA chain movement. The Figure 4b illustrates

the storage modulus with the addition of MAH in 20%WCF–PLA. The addition of 3%MAH enhances the storage modulus upto 10% in comparison to MAH free WCF–PLA composite. The enhancement of storage modulus indicates the improvement in thermomechanical characteristics. The results correspond to the findings of Zhang [39] which showed that the storage modulus of PLA/WF/MAH composite was 4.06 GPa. The introduction of MAH initiates a formation of stronger structure due to the interfacial adhesion between WCF and PLA matrix. The improvement in interfacial adhesion helps to dissipate the externally applied load uniformly from PLA matrix to WCF fiber preserving the integrity of structure and enhancing the toughness of the composite. The similar effect has been found in 10%WCF–PLA–MAH and 30%WCF–PLA–MAH. The storage modulus values for PLA, PLA/WCF, and PLA/WCF/WCF are presented in Table 2.

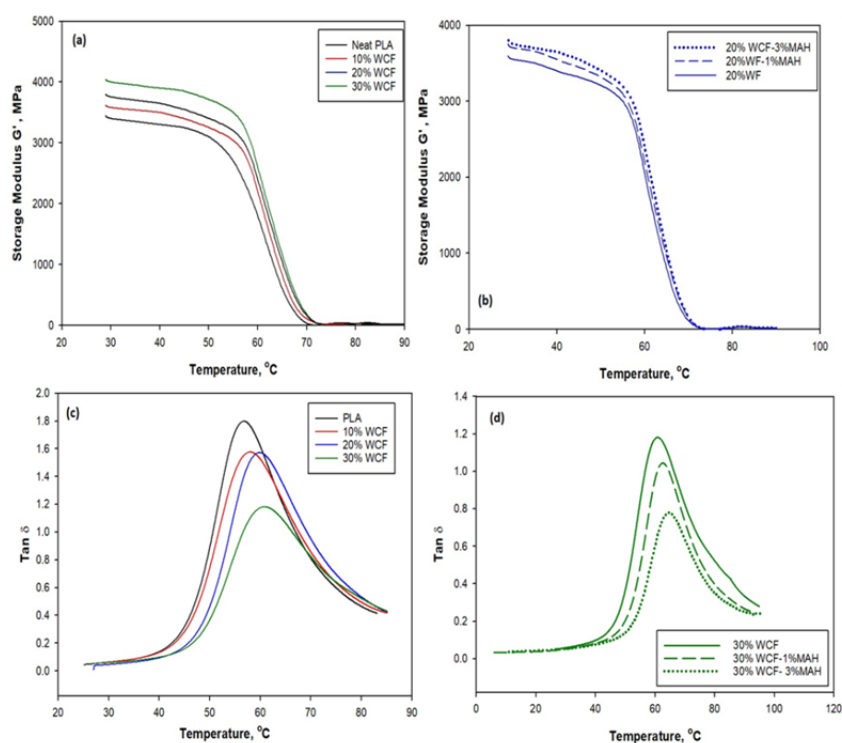


Figure 4. Dynamic mechanical thermal analysis (a) storage modulus of WCF–PLA, (b) storage modulus of WCF–PLA–MAH, (c) $\tan \delta$ of WCF–PLA, and (d) $\tan \delta$ of 30%WCF–PLA–MAH.

The variation of loss factor $\tan \delta$ is shown in Figure 4c with respect to temperature for neat PLA and WCF–PLA composite. The Figure 4c presents that the addition of 30%WCF in PLA reduces the height of $\tan \delta$ peak from 1.81 to 1.21 which is due to the restriction of polymer molecules movement by the addition of wood cellulose fiber. The Figure 4d and Table 2 shows that the peak height shrank to 0.81 with the addition of 3% MAH in 30%WCF–PLA indicating the improvement in interfacial adhesion. Also, Huda et al [41] concluded that the height of $\tan \delta$ peak decreases up to 1.01 due to the addition of 30%WCF in PLA matrix. The drop in $\tan \delta$ peak results in increase of molecular relaxation and stronger interfacial adhesion which in turn assists the WCF–PLA composite to endure significant amount of energy. A similar impact has been shown by 10%WCF–PLA and 20%WCF–PLA with the addition of MAH as presented in Table 2.

Furthermore, $\tan\delta$ peak position defines the glass transition temperature T_g changes and results are indicated in Table 2. The glass transition temperature T_g of 30%WCF–PLA is 59.98 °C which is higher when compared to neat PLA. The rise in T_g occurs due to the addition of WCF which restricts the motion of PLA molecule in the composite. Zhang et al. [39] found the T_g of 30%WF–PLA around 62.3 °C which is 3% higher than the presented findings. Additionally, the use of MAH as coupling agent caused the glass transition temperature to increase up to 61.76 °C as shown in Figure 4d and Table 2 for 30%WCF–PLA. The increase in glass transition temperature T_g shows that the suitable interfacial bonding occurred between WCF and PLA. Also, similar effect has been found for 10%WCF–PLA and 20%WCF–PLA with the addition of MAH as shown in Table 2.

The relative damping of the polymer matrix and composite can be applied to calculate the adhesion factor A by utilizing the volume fraction of fiber as shown in Eq 2 [42]:

$$A = \frac{1}{(1-V_f)} \frac{\tan\delta_c}{\tan\delta_p} - 1 \quad (2)$$

The $\tan\delta_p$ and $\tan\delta_c$ are the relative damping of polymer and composite while V_f is the volume fraction of fiber.

As shown in Table 2, the Adhesion factor A decreases with the addition of MAH in WCF–PLA composite. The 30%WCF–PLA exhibits the minimum adhesion factor which is -0.61 . The lower value of adhesion factor A can be attributed to strong adhesion and decrease in reduction in $\tan\delta_c$. The reduction in molecular mobility causes decrease in $\tan\delta_c$ which in turn improves the interfacial interaction between WCF and PLA matrix. The increase in interfacial interaction has strong impact on the characteristics such as mechanical and thermomechanical properties of WCF–PLA composite as shown in Figures 2 and 4.

3.4. Orientation of fiber

The Figure 5 shows X-ray tomography segmented images of 10%, 20%, 30%WCF–PLA–MAH composite and core shell of 20%WCF–PLA–MAH composite which shows fiber dispersion and orientation. The core and shell corresponds to the center and surface of segmented volume of specimen as shown in Figure 5d.

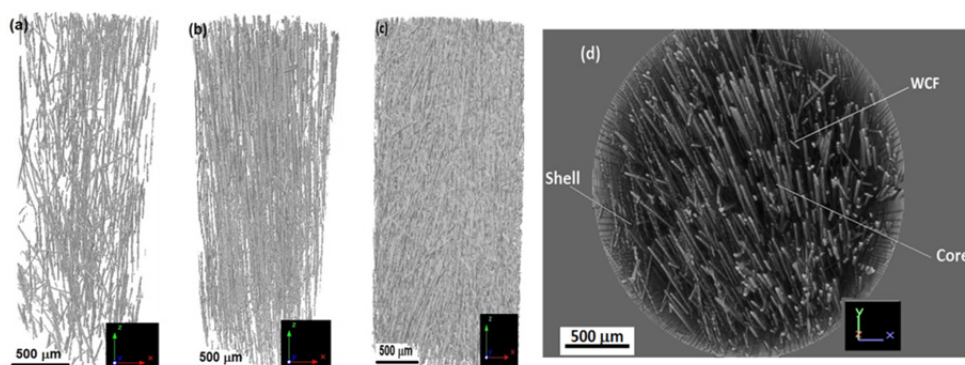


Figure 5. Cross section of wood fiber images (voxel size = 10 μm) (a) side view of 10% WCF, (b) side view of 20% WCF, (c) side view of 30% WCF, and (d) top view-core-shell structure of 20%WCF–PLA–3%MAH.

The Figure 6a illustrates the orientation variation between 10%, 20% and 30% WCF in PLA matrix when 3%MAH is being added. In addition, Figure 6a shows that 40–45% of fibers in PLA composite containing 30% wood cellulose fibers are in the direction of 0° and 180° (Z axis) when compared to composite of 10% and 20% WCF reinforced PLA. The outcome defines that during the process of compression molding the randomness of fiber increases with the decrease of fiber content. The randomness in composite might be because of the variation of flow velocity of fiber in PLA that cause the entanglement of fiber with non-homogeneous dissemination in PLA composite. The calculated orientation data is being presented in Figure 6b illustrating the axis for the wood cellulose fiber content and a_{ij} components of tensor. The a_{33} component (Z axis) of the tensor is 0.70 in 30%WCF–PLA which is higher than the 10% and 20% WCF reinforcement. The variation in the a_{ij} components values is due to the viscosity and shear stresses during compression that directs the WCF to be oriented in machine direction. The Z axis (0° and 180°) follows the a_{33} component which corresponds to compression molding machine direction. Meanwhile, a_{22} and a_{11} components follow the normal and transverse direction. The data presents that the higher amount of fibers directed towards the a_{33} components. The orientation of fiber increases in the flow direction with the increase of fiber content which is also presented by Neves et al. [43] in GF reinforced polypropylene composite.

The degree of anisotropy (DA) is a calculation of orientation of fibers within a specified volume. The calculated values for DA change from 1 which is isotropic to infinity which is completely anisotropic and can be calculated by Eq 3 [44]:

$$DA = \left[1 - \left(\frac{\text{MinimumEigenvalue}}{\text{MaximumEigenvalue}} \right) \right] \quad (3)$$

Figure 6c demonstrates the degree of anisotropy (DA) at 0.52 ± 0.04 for 30%WCF–PLA–3%MAH composite which is higher when compared to 0.32 ± 0.02 for 10% reinforcement. Similar trend in the degree of anisotropy can be observed in MAH free WCF–PLA indicating that the addition of maleic anhydride (MAH) has no impact on the degree of anisotropy. Furthermore, 10%WCF–PLA–MAH composite presents that the higher amount of fiber is directed towards the transverse and normal orientation along the X and Y axis representing a non uniform dispersion [44]. In 30% WCF composite the significant fibers directs and flows toward Z axis which is related to a_{33} components and corresponds to machine direction presenting uniform dispersion of WCF in PLA matrix. Also, the uniform dispersion of 30% WCF in PLA corresponds to the increase in strength, elastic modulus and storage modulus. Figure 6d illustrate the core-shell effect in the WCF–PLA–MAH composite. The degree of anisotropy (DA) in the core of 20%WCF–PLA is 0.55 ± 0.015 which is higher when compared to shell which is 0.21 ± 0.037 indicates fiber orientation occurred during compression molding. The degree of anisotropy (DA) in the core of 30%WCF–PLA and 10%WCF–PLA is 0.61 ± 0.025 and 0.42 ± 0.022 which are higher than the shell. The alignment of fibers in the core follows the shear flow which orientates the WCF fiber to the direction of PLA flow corresponds to Z direction. Furthermore, the alignment of fibers in the shell follows the extensional flow which orientates the WCF fiber perpendicular to the direction of PLA flow. Bernasconi et al. [45] by using X-ray tomomography found the similar effect for injection molded glass fiber reinforced polyamide composite. The results show the higher DA of the core has strong influence in increasing the strength, elastic modulus and storage modulus of the WCF–PLA composite.

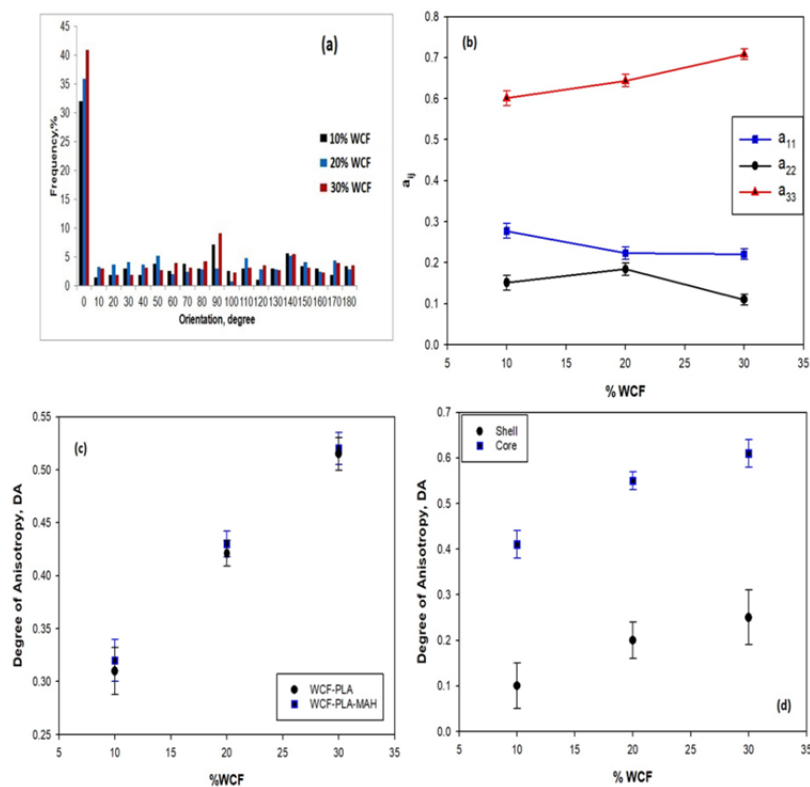


Figure 6. (a) Wood cellulose fiber orientation in PLA matrix, (b) orientation components a_{11} , a_{22} and a_{33} with respect to wood cellulose fibers concentration (error bars: three test of same compositions), (c) degree of Anisotropy with respect to wood cellulose fibers concentration (error bars: three test of same compositions), and (d) degree of anisotropy of core-shell section in 20%WCF-PLA-3%MAH.

3.5. Fracture surface

The Figure 7 shows the fracture surface of WCF/PLA/MAH composite. In the Figure 7a the smooth and leveled fracture surface of neat PLA can be seen which indicates negligible deformation. The Figure 7b shows the fracture surface of PLA/WCF composite without the addition of MAH. The phase separation between PLA matrix and WCF can be noticed having rough surface including voids. The tensile strength examination shows that WCF can be pulled out from PLA matrix presenting the inadequate interfacial adhesion. It is evident from Figure 7c that the decrease of voids occurred with the addition of 3%MAH in WCF-PLA composite. The reduction in WCF extraction preserves the strong interfacial adhesion with PLA matrix that can sustain the higher load. The Figure 7d shows the initiation of strain in the single fiber presenting the fracture of wood cellulose fiber in PLA/20%WCF/MAH composite. The effect of MAH addition is evident in the improvement of adhesion and interfacial bonding which shows the load transfer from PLA matrix to wood cellulose fiber. Moreover, the MAH addition produces significant compatibility and interfacial integrity between WCF and PLA matrix. The evidence of enhanced storage modulus and improved mechanical properties shows the benefit of adding MAH as coupling agent in the WCF-PLA composite.

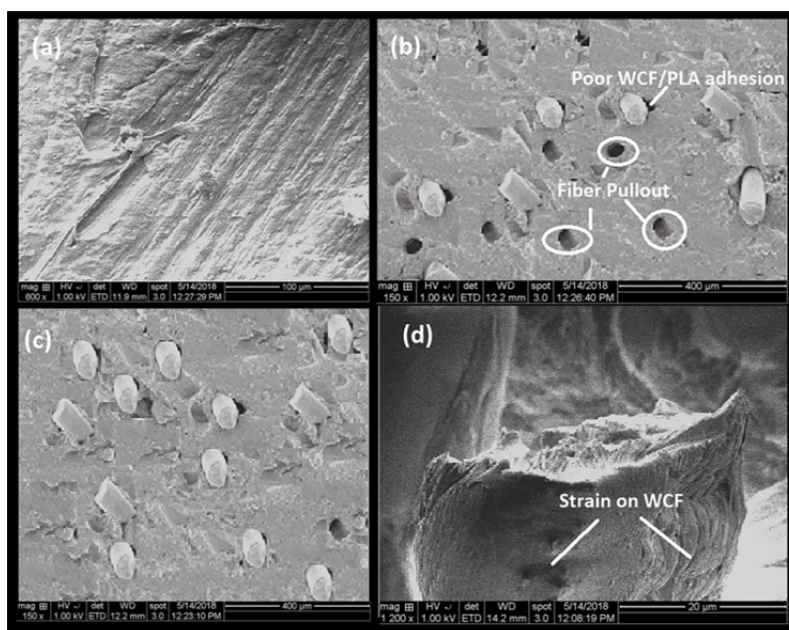


Figure 7. SEM micrograph of fracture surface (a) Neat PLA, (b) 20%WCF–PLA, (c) 20%WCF–PLA–3%MAH, and (d) strain on single WCF.

4. Conclusion

The WCF reinforced PLA with the addition of MAH was blended by using twin screw extruder and was successfully compression molded. The mechanical properties, thermomechanical properties, orientation of WCF in PLA matrix and interfacial compatibility were investigated by adding varying amounts of MAH in WCF–PLA composite. Also, MAH acted as an interfacial coupling agent in WCF–PLA composite which appear to be beneficial in improving toughness, elastic modulus and impact strength. The enhancement in mechanical properties created a composite which is tougher when compared to MAH free composite. The addition of 3%MAH provided suitable results in the form of reduced $\text{Tan}\delta$ peak and increased glass transition temperature T_g which also indicates improvement in interfacial adhesion between WCF and PLA matrix. The degree of anisotropy is found to be higher in 30%WCF/PLA when compared to 10%WCF–PLA and 20%WCF–PLA. The 30%WCF–PLA composite is isotropic due to higher degree of anisotropy which in turn enhanced the mechanical and thermomechanical properties of WCF-PLA composite. The fracture surface shows significant reduction in voids in the WCF–PLA composite with the addition of MAH. Finally, the fracture surface illustrates that the addition of MAH improved the interfacial adhesion between WCF and PLA matrix resulting in a tougher WCF–PLA–MAH composite.

Acknowledgements

The Author would like to extend his gratitude to Chemical & Materials Engineering Department, King Abdulaziz University Jeddah for supporting this research.

Conflict of interest

No conflict of interest needs to declare.

References

1. Dittenber DB, GangaRao HV (2012) Critical review of recent publications on use of natural composites in infrastructure. *Compos Part A-Appl S* 43: 1419–1429.
2. Ashori A (2008) Wood-plastic composites as promising green-composites for automotive industries. *Bioresource Technol* 99: 4661–4671.
3. Sanyang ML, Illyas RA, Saupen SM, et al. (2018) Sugar palm starch-based composites for packaging applications, In: Jawaid M, Swain SK, *Bionanocomposites for Packaging Applications*, Springer-Cham, 125–147.
4. Lavoine N, Dufresne A, Desloges I, et al. (2012) Microfibrillated cellulose-its barrier properties and applications in cellulosic materials: A review. *Carbohyd Polym* 90: 735–764.
5. Khalil HPSA, Yusra AF (2012) Green composites from sustainable cellulose nanofibrils: A review. *Carbohyd Polym* 87: 963–974.
6. Xu SY, Xie YZ, Meng LX (2016) Application of biomass-based composites in food packaging. *For Eng* 32: 85–89.
7. Armentano I, Bitinis N, Fortunati E, et al. (2013) Multifunctional nanostructured PLA materials for packaging and tissue engineering. *Prog Polym Sci* 38: 1720–1747.
8. Torres J, Cotelo J, Karl J, et al. (2015) Mechanical property optimization of FDM PLA in shear with multiple objectives. *JOM* 67:1183–1193.
9. Hsieh CT, Pan YJ, Lou CW, et al. (2016) Polylactic acid/carbon fiber composites: effects of functionalized elastomers on mechanical properties, thermal behavior, surface compatibility, and electrical characteristics. *Fiber Polym* 17: 615–623.
10. Yusoff RB, Takagi H, Nakagaito AN (2016) Tensile and flexural properties of polylactic acid-based hybrid green composites reinforced by kenaf, bamboo and coir fibers. *Ind Crop Prod* 94: 562–573.
11. Panthapulakkal S, Law S, Sain M (2005) Enhancement of processability of rice husk filled high-density polyethylene composite profiles. *J Thermoplas Compos Mater* 18:445–450.
12. Mohanty S, Verma SK, Nayak S (2006) Dynamic mechanical and thermal properties of MAPE treated jute/HDPE composite. *Compos Sci Technol* 66: 538–543.
13. Li X, Tabil LG, Oguocha IN, et al. (2008) Thermal diffusivity, thermal conductivity, and specific heat of flax fiber-HDPE biocomposites at processing temperature. *Compos Sci Technol* 68: 1753–1758.
14. Semeralul HO, Rizvi GM (2008) Glass fiber reinforced wood/plastic composites. *J Vinyl Addit Techn* 14: 39–42.
15. Guo G, Lee YH, Rizvi GM, et al. (2008) Influence of wood fiber size on extrusion foaming of wood fiber/HDPE composites. *J Appl Polym Sci* 107: 3505–3511.
16. Porrás A, Marañón A, Ashcroft IA (2015) Characterization of a novel natural cellulose fabric from *Manicaria saccharifera* palm as possible reinforcement of composite materials. *Compos Part B-Eng* 74: 66–73.

17. Nakagaito A, Yano NH (2005) Novel high-strength biocomposites based on microfibrillated cellulose having nano-order unit web-like network structure. *Appl Phys A-Mater* 80: 155–159.
18. Gupta A, Simmons W, Schueneman GT, et al. (2016) Lignin-coated cellulose nanocrystals as promising nucleating agent for poly(lactic acid). *JTAC* 126: 1243–1251.
19. Ilyas RA, Sapuan SM, Ishak MR, et al. (2019) Sugar palm nanofibrillated cellulose: effect of cycles on their yield, physic-chemical, morphological and thermal behavior. *Int J Biol Macromol* 123: 379–388.
20. Ilyas RA, Sapuan SM, Sanyang ML, et al. (2018) Nanocrystalline cellulose as reinforcement for polymeric matrix nanocomposites and its potential applications: a review. *Curr Anal Chem* 14: 203–225.
21. Qin J, Jiang Y, Fu J, et al. (2013) Evaluation of drug release property and blood compatibility of aspirin-loaded electrospun PLA/RSF composite nanofibers. *Iran Polym J* 22:729–737.
22. Guo W, Ashida M (1993) Mechanical properties of PET short fiber-polyester thermoplastic elastomer composites. *J Appl Polym Sci* 50: 1435–1443.
23. Saeed U, Dawood U, Ali AM (2019) Cellulose triacetate fiber-reinforced polystyrene composite. *J Thermoplast Compos* 2: 1–15.
24. George J, Shreekala MS, Thomas S (2001) A review on interface modification and characterization of natural fibre reinforced plastic composites. *Polym Eng Sci* 41: 1471–1485.
25. Saba N, Jawaid M, Othman Y, et al. (2016) A review on dynamic mechanical properties of natural fibre reinforced polymer composites. *Constr Build Mater* 106: 149–159.
26. Huang H, Zhang J (2009) Effects of filler-filler and polymer-filler interactions on rheological and mechanical properties of HDPE-wood composites. *J Appl Polym Sci* 111: 2806–2813.
27. Kirz J, Jacobsen C, Howells M (1995) Soft X-ray microscopes and their biological applications. *Q Rev Biophys* 28: 33–130.
28. Ritman EL (2002) Molecular imaging in small animals-roles for micro-CT cell. *J Cell Biochem* 87: 116–120.
29. Kak AC, Slaney M (1988) *Principles of Computerized Tomographic Imaging*, New York: The Instbte of Electrical and Electronics Engineers.
30. Pandita SD, Verpoest I (2003) Prediction of the tensile stiffness of weft knitted fabric composites based on X-ray tomography images. *Compos Sci Technol* 63: 311–325.
31. Faessel M, Delisee C, Bos F, et al. (2005) 3D modelling of random cellulosic fibrous networks based on X-ray tomography and image analysis. *Compos Sci Technol* 65: 1931–1940.
32. Schilling, PJ, Kadedla BR, Tatiparthi AK, et al. (2005) X-ray computed microtomography of internal damage in fiber reinforced polymer matrix composites. *Compos Sci Technol* 65: 2071–2078.
33. Eichhorn SJ, Baillie CA, Zafeiropoulos N, et al. (2001) Review: current international research into cellulosic fibres and composites. *J Mater Sci* 36: 2107–2131.
34. Hrabalova M, Gregorova A, Wimmer R, et al. (2010) Effect of wood flour loading and thermal annealing on viscoelastic properties of PLA composite films. *J Appl Polym Sci* 118: 1534–1540.
35. Ekevad M (2004) Method to compute fiber directions in wood from computed tomography images. *J Wood Sci* 50: 41–45.
36. Walther T, Terzic K, Meine H, et al. (2006) Microstructural analysis of lignocellulosic fiber networks. *Developments in X-ray Tomography V* 6318: 631812.

37. Saeed U, Rizvi G (2015) Three dimensional orientation of compression-molded high density polyethylene/wood fibers using X-ray micro-tomography. *J Cell Plast* 51: 45–57.
38. Way C, Wu DY, Palombo E, et al. (2012) Processing stability and biodegradation of polylactic acid (PLA) composites reinforced with cotton linters or maple hardwood fibres. *J Polym Environ* 21: 54–70.
39. Zhang L, Lv S, Sun C, et al. (2017) Effect of MAH-g-PLA on the properties of wood fiber/polylactic acid composites. *Polymers* 9: 591.
40. Saeed U, Hussain K, Rizvi G (2014) HDPE reinforced with glass fibers: rheology, tensile properties, stress relaxation, and orientation of fibers. *Polym Composite* 35: 2159–2169.
41. Huda MS, Drzal LT, Mohanty AK, et al. (2006) Wood fiber reinforced polylactic acid composite: evaluation of the physicomechanical and morphological properties. *J Appl Polym Sci* 102: 4856–4869.
42. Correa CA, Razzino CA, Hage JE (2007) Role of maleated coupling agents on the interface adhesion of polypropylene-wood composites. *J Thermoplast Compos* 20: 323–339.
43. Neves NM, Pontes AJ, Pouzada, AS (2002) Fiber contents effect on the fiber orientation in injection molded GF/PP composites plates. *Society of Plastic Engineering (SPE) ANTEC*.
44. Cosmi F, Bernasconi A, Sodini N (2011) Phase contrast micro-tomography and morphological analysis of a short carbon fibre reinforced polyamide. *Compos Sci Technol* 71: 23–30.
45. Bernasconi A, Cosmi F, Dreossi D (2008) Local anisotropy analysis of injection moulded fibre reinforced polymer composites. *Compos Sci Technol* 68: 2574–2581.



AIMS Press

©2020 the Author(s), licensee AIMS Press. This is an open access article distributed under the terms of the Creative Commons Attribution License (<http://creativecommons.org/licenses/by/4.0>)